Nanoscale

COMMUNICATION

View Article Online
View Journal | View Issue

Cite this: *Nanoscale*, 2026, **18**, 159

Received 1st September 2025,
Accepted 1st December 2025

DOI: 10.1039/d5nr03695j

rsc.li/nanoscale

On the role of cation–DNA interactions in surface-assisted DNA lattice assembly

Xiaodan Xu,[a] Bhanu Kiran Pothineni,†[a] Guido Grundmeier,[a] Satoru Tsushima *[b,c] and Adrian Keller *[a]

Surface-assisted DNA lattice assembly is used in the synthesis of functional surfaces and as a model of supramolecular network formation. Here, competitive DNA binding of different cation species is investigated by molecular dynamics simulations and correlated with experiments of surface-assisted DNA origami lattice assembly. The results demonstrate that cation–DNA binding has a strong impact on lattice assembly and order.

The surface-assisted assembly of DNA lattices is an emerging technology with important applications in materials science. Such lattices are used as templates for the ordered arrangement of nanoparticles and proteins[1–4] and as masks in molecular lithography.[5] Furthermore, surface-assisted DNA lattice assembly also serves as a model system for unravelling the fundamental mechanisms that govern the formation of supramolecular networks and crystals.[6,7] Therefore, numerous variants of surface-assisted DNA lattice assembly have been reported using small DNA tiles[2,5–10] and large DNA origami nanostructures[3,4,11–21] at mica[2–4,6–16,20] and SiO_2 surfaces[5,17–19,21] with[2–10,14,15,19] or without[11–13,15–18,20,21] attractive interactions between individual nanostructures.

Despite this great variety, DNA lattice assembly in all its implementations relies on the same molecular mechanism. Since both mica and SiO_2 surfaces are negatively charged at neutral and basic pH, adsorption of negatively charged DNA nanostructures is facilitated by divalent cations such as Mg^{2+}, which form salt bridges between negatively charged surface sites and the negatively charged phosphate groups in the DNA backbone. To facilitate the assembly of the adsorbed DNA nanostructures into ordered lattices, the strength of the interaction between DNA and surface must be fine-tuned to allow lateral diffusion of the DNA nanostructures while keeping them confined to the surface. Depending on the actual system, this may require an adjustment of the divalent cation concentration,[2,6,8,22] elevated substrate temperature,[10,14,17–19,23] externally applied potentials,[21] and/or the addition of monovalent cations[1,3–6,11–22] such as Na^+. In the latter case, the monovalent cations replace some of the adsorbed divalent cations, thereby reducing the number of salt bridges.

Additionally, a few studies reported that also the cation species has an effect on DNA lattice assembly and especially lattice order.[6,12,17] For non-interacting DNA origami triangles at mica surfaces, notably lower lattice order was obtained for both Li^+ and especially K^+ than for Na^+ when combined with Mg^{2+}.[12] Furthermore, replacing Mg^{2+} with Ca^{2+} in the presences of Na^+ led to an increase in lattice order.[12] Interestingly, the same was observed also at SiO_2 surfaces, which require much higher Na^+ concentrations in combination with elevated substrate temperatures for lattice assembly.[17] Recently, improved lattice order in the presence of Ca^{2+} compared to Mg^{2+} was also reported for the assembly of small, interacting DNA tiles at mica without any monovalent cations.[6]

The origin of this cation dependence is still a matter of speculation.[6,12,17] In general, there are two mechanisms that may contribute to this effect. First, different divalent cations may interact differently with the surface. However, previous studies observed similar cation dependencies on mica and SiO_2 surfaces,[6,12,17] which rather suggests a surface-independent mechanism. This is further supported by other studies showing that Mg^{2+} and Ca^{2+} are rather similar in their interactions with mica surfaces.[24,25] In addition, at a pH around 8 as commonly used in surface-assisted DNA lattice assembly, the ζ potential of mica surfaces adopts almost identical values in contact with both Mg^{2+} and Ca^{2+} at the same concentrations.[26] The same is observed also for SiO_2 surfaces.[27] The second mechanism assumes differences in the interaction of Mg^{2+} and Ca^{2+} with DNA. While previous studies have specu-

[a]*Paderborn University, Technical and Macromolecular Chemistry, Warburger Str. 100, Paderborn 33098, Germany. E-mail: adrian.keller@uni-paderborn.de*
[b]*Helmholtz-Zentrum Dresden-Rossendorf, Institute of Resource Ecology, Bautzner Landstrasse 400, Dresden 01328, Germany. E-mail: s.tsushima@hzdr.de*
[c]*Laboratory for Zero-Carbon Energy, Institute of Science Tokyo, Tokyo 152-8550, Japan*
† Present address: Programmable Biomaterials Laboratory, Institute of Materials, School of Engineering, École Polytechnique Fédérale de Lausanne, Lausanne 1015, Switzerland.

lated how such differences might affect surface-assisted DNA lattice assembly,[6,12,17] the molecular details are not understood yet. This is mostly because of the complexity of the system, which is based on the competitive binding of different concentrations of monovalent and divalent cations to compact DNA nanostructures that may exhibit a variety of different DNA conformations.

In this work, we aim to shed some light on the role of cation–DNA interactions in surface-assisted DNA lattice assembly by analyzing DNA–cation interactions in a simplified model system using molecular dynamics (MD) simulations and correlating the obtained results with atomic force microscopy (AFM) investigations of DNA origami lattice assembly at mica surfaces. Even though several substantial simplifications are introduced in the MD simulations, the computational results correlate very well with the experimental observations, providing clear evidence for cation–DNA binding being a dominant mechanism in surface-assisted DNA lattice assembly. Furthermore, our results suggest that straightforward and computationally rather inexpensive MD simulations can be used to screen various cation combinations for their potential to stimulate the assembly of highly ordered DNA lattices at solid surfaces. This is demonstrated using Sr^{2+} as a test case, as this cation has not been explored in surface-assisted DNA lattice assembly yet.

A number of previous studies have used molecular-level simulations to gain insight into the roles of different cations in DNA assembly. These works focused on the interaction of DNA with lipids[28,29] and DNA–DNA interactions.[30–33] In the present study, the emphasis was placed on the examination of the competitive binding of monovalent and divalent cations to DNA. For this purpose, a simplified system was selected comprising a single DNA molecule in conjunction with a series of monovalent and divalent cations. By making the following assumptions and simplifications, these cation–DNA interactions could be investigated at reasonable computational cost.

First, the MD simulations were performed using a Dickerson-Drew B-DNA dodecamer as a model for DNA. This simple duplex DNA was selected because DNA origami adsorption at mica and SiO_2 surfaces involves only those ions bound to phosphate groups located on the DNA origami surface but not those between neighboring double helices. In addition, the lattice system investigated in our experiments below does not involve attractive interactions such as blunt-end stacking or sticky-end hybridization between the DNA origami nanostructures. Attractive electrostatic interactions due to DNA-bound divalent cations can be ruled out as well, as those would lead to notable DNA origami aggregation at the surface[12] or even in bulk solution.[34] Rather, lattice formation results solely from electrostatic interactions between the DNA origami nanostructures and the mica surface. Therefore, there is no need to simulate larger assemblies of laterally interacting duplexes.

Second, the dodecamer was exposed to a mixture of monovalent (Na^+/K^+) and divalent ($Mg^{2+}/Ca^{2+}/Sr^{2+}$) cations at a 9 : 1 ratio, corresponding to 18 and 2 M^+ and M^{2+} ions, respectively. While this ratio is similar to the ratios employed in DNA origami lattice assembly at mica surfaces,[1,3,11–13,15,16,20] the ratio of cations to DNA base pairs is three to four orders of magnitude lower than in typical experiments, which usually use mM concentrations of divalent cations and μM concentrations of DNA base pairs. Although this will leave many potential cation binding sites in the DNA unoccupied, differences in cation binding will become more visible.

Third, instead of monitoring the initial interactions of divalent cations with DNA, we started the simulations with an M^{2+}-bound state in which the divalent cations were placed in the vicinity of their known binding sites (*i.e.*, the phosphate groups) and studied their dynamics in the presence of an excess of monovalent cations. This is equivalent to the DNA nanostructures being stored for extended periods of time (minutes to hours) in M^{2+}-containing buffer prior to lattice assembly and thus in line with our experimental approach.

Fourth, the MD simulation was conducted for a duration of 200 ns for each system under investigation. The analysis was confined to solely the latter half of the MD trajectory, which corresponded to 100 ns. This methodological decision was made with the objective of ensuring that the system had attained sufficient equilibrium. For each system, three replicas of simulations were generated, resulting in a total simulation time of 300 ns. Two divalent cations were positioned at the center of the DNA within the minor grove (named simulation A). However, for the system including Mg^{2+}, where the mobility of divalent cations is low, a second set of simulations was also performed (named simulation B), placing the two Mg^{2+} at the edge of the DNA in the major groove.

Of the three divalent ions under consideration, Mg^{2+} is the sole ion found to be stably bound to the phosphate group of the DNA, remaining practically immobile during the 300 ns simulation, regardless of the type of simulations (A and B). The phosphate oxygen atoms within a 3 Å radius of the Mg^{2+} ion exhibit an average coordination number of 4.000 and 2.000, respectively, for simulation A and B. The two Mg^{2+} ions exhibit distinct coordination patterns for simulation A: one Mg^{2+} ion is coordinated bidentately by a single phosphate group, while another Mg^{2+} ion exhibits coordination from two different phosphate groups through interstrand crosslinking. For simulation B, both Mg^{2+} ions coordinate monodentately to single phosphate groups. Clearly, Mg^{2+} binding is not site-specific, and their positions are determined by their initial positions, although their positions may change over time. The observation of Mg^{2+} coordination to the phosphate groups in DNA is consistent for both Na^+ and K^+. In Fig. 1A and B, DNA and Mg^{2+} are depicted as white ribbon and blue balls, respectively, in superimposed MD snapshots at every 1 ns of the 100 ns MD trajectory (only shown for the first 100 ns simulation). The fluctuation of the DNA structures and the positions of the Mg^{2+} ions is evident; nevertheless, the divalent ions remain essentially at the same position relative to the DNA. In contrast, a clear distinction emerges in the proximity of the base pairs, where the association of monovalent ions to the base

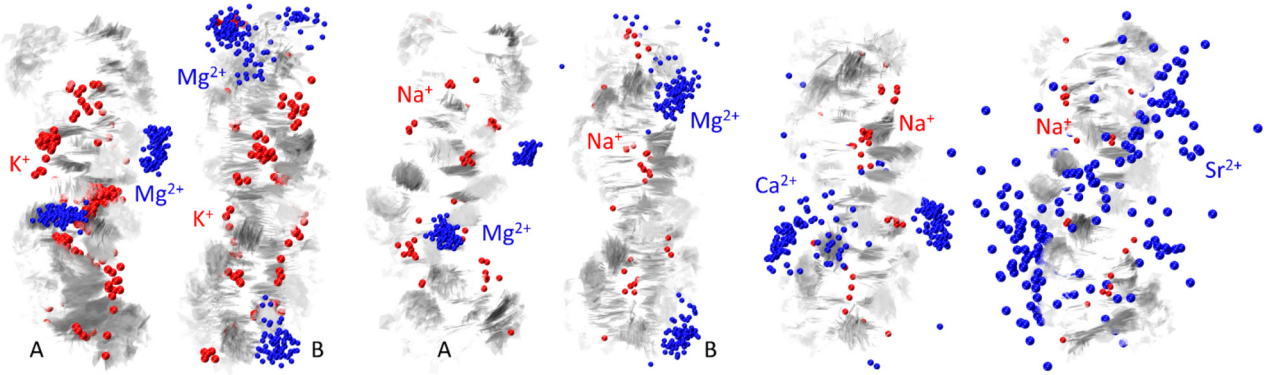

Fig. 1 Superposition of 100 snapshots from the MD trajectory showing cation-specific differences in DNA binding. From left to right: Mg^{2+}/K^{+} (for simulations A and B), Mg^{2+}/Na^{+} (for simulations A and B), Ca^{2+}/Na^{+}, and Sr^{2+}/Na^{+}. DNA is depicted as a gray ribbon, whereas monovalent and divalent cations are shown as red and blue balls, respectively.

pairs' oxygen and nitrogen atoms is observed. K^{+} ions exhibit a stronger association with oxygen at a distance >2.5 Å, whereas such association is clearly weaker in the case of Na^{+} (Fig. S1). Also, the three simulation series show more distinct variations in the Na^{+} series compared to the K^{+} series, due to their weaker associations. In Fig. 1, monovalent ions are represented by red spheres, for which only those within 3 Å of base pair O are plotted. The number of red spheres for Mg^{2+}/Na^{+} is significantly reduced compared to Mg^{2+}/K^{+}, as there are fewer monovalent cations in the vicinity of the base pairs for Na^{+} compared to K^{+}. At the same time, K^{+} has a lower average coordination number to phosphate (1.403) than Na^{+} (1.586, see Table S1). These observations indicate that Na^{+} has a higher propensity to compete with Mg^{2+} for binding to the backbone phosphates, while K^{+} ions demonstrate a higher tendency to bind to the surface of DNA, thereby rendering it electrically neutral; a trend that is less pronounced in the case of Na^{+}. Therefore, the observed differences in the association of K^{+} and Na^{+} with DNA suggest that Na^{+} is superior in increasing the surface mobility of adsorbed DNA origami nanostructures, whereas K^{+} has a higher tendency to contribute to DNA aggregation and thereby hinder DNA lattice assembly as observed in previous experiments.[12]

Cheng *et al.* studied the influence of K^{+} and Na^{+} binding to DNA also by MD simulations and concluded that K^{+} ions bind to the electronegative sites of DNA bases in the major and minor grooves, while Na^{+} ions interact preferentially with the phosphate groups.[35] The findings by Cheng *et al.* are consistent with the current MD results. The observed preference for K^{+} over Na^{+} in DNA has previously been interpreted as being due to the higher energy cost of dehydrating Na^{+} compared to K^{+}.[36] It is known that the hydration energy of monovalent alkali metal cations increases with decreasing atomic number due to their decreasing size, being highest for Li^{+}. The Gibbs free energy of hydration at 298.15 K is −365 and −295 kJ mol^{-1} for Na^{+} and K^{+}, respectively.[37] Nucleobases do not correspond to hard bases in a classical sense, and they exhibit a stronger association with softer acids, such as K^{+}, as opposed to Na^{+}. The observed behaviors of Na^{+} and K^{+} thus align with the prevailing chemical understanding concerning these ions.

Next, we focused on the effect of the difference in divalent cations, namely the difference amongst Mg^{2+}, Ca^{2+}, and Sr^{2+}. While Mg^{2+} and Ca^{2+} are frequently employed in DNA lattice assembly, Sr^{2+} has not been explored in this context yet. Therefore, we selected this cation as a novel test case for our MD simulations. We substituted Mg^{2+} with Ca^{2+} and Sr^{2+}, while maintaining a constant ratio of monovalent to divalent cations of 9. To assess the impact of these alterations, we conducted simulations on the monovalent cations, both Na^{+} and K^{+}. This has led to the generation of six sets of simulations, each focusing on a specific pairing of Na^{+}/K^{+} with $Mg^{2+}/Ca^{2+}/Sr^{2+}$. The phosphate oxygen atoms within a 3 Å radius of the Ca^{2+} ion throughout the MD trajectory exhibit average coordination numbers of 1.812 and 1.801 for Na^{+} and K^{+}, respectively, which are significantly reduced compared to 4.000 for Mg^{2+}. This number decreases further for Sr^{2+}, reaching 0.818 and 0.934 for Na^{+} and K^{+}, respectively. These decreases in the M^{2+} coordination numbers are accompanied by increases in the M^{+} coordination numbers (Table S1), indicating stronger replacement of phosphate-bound M^{2+} by M^{+}. The results suggest that Ca^{2+} and Sr^{2+} exhibit significantly reduced binding affinity for DNA, indicating that the divalent cation substitution exerts dual effects on M^{2+} coordination to phosphate and on M^{2+} mobility. In Fig. 1, the distributions of Ca^{2+} and Sr^{2+} ions are plotted for each 1 ns of the 100 ns MD trajectory. These demonstrate that these two cations exhibit greater mobility compared to Mg^{2+}. Consequently, an increased number of M^{2+} cations are observed in the proximity of the base pairs of the DNA, though at a distance that prevents direct interaction with the oxygens of the base pairs. Instead, these divalent cations appear to "purge" and replace Na^{+} and K^{+} that are weakly associated with N atoms of the base pairs. However, it is evident from the distributions of Ca^{2+} and Sr^{2+} in Fig. 1 that these cations are not consistently associated with any specific sites. It is also important to note that such a trend is difficult to detect from a single MD snapshot, and that stat-

istical analysis is essential. This is illustrated in Fig. S2, where the results from different simulations are presented, though the distinctions between them are not apparent. Furthermore, a clear trend indicates that DNA exhibits reduced association with cations when transitioning from K^+ to Na^+ and from Mg^{2+} to Ca^{2+} and to Sr^{2+}. Reduced association of Ca^{2+} with the backbone phosphates has previously been postulated as a possible origin of the observed increase in DNA lattice order when replacing Mg^{2+} with Ca^{2+}.[6,12,17]

While the trends observed in the MD simulations qualitatively agree with previous observations, we aimed for a more direct verification and monitored the adsorption and assembly of non-interacting triangular DNA origami nanostructures[38] at mica surfaces at the same ratio of monovalent to divalent cations, *i.e.*, 10 mM M^{2+} and 90 mM M^+, which has not been studied previously. Interestingly, for all divalent cations, lattices are obtained in the presence of Na^+, whereas K^+ always leads to the formation of disordered multilayers (see Fig. 2). This is in agreement with the behavior observed in Fig. 1A, where the collective binding of Mg^{2+} and K^+ contributes more strongly to charge neutralization and possibly even a partial charge inversion of the DNA and thereby promotes DNA aggregation. In the case of Na^+ (Fig. 1B), binding to the nucleobases is strongly reduced and this effect therefore less pronounced.

The species of the divalent cation has a more subtle effect on lattice assembly. While the overall time course of adsorption and lattice assembly is largely unaffected by the species of the divalent cation (see Fig. S3–S8), the lattices formed in the presence of Na^+ exhibit some visible differences. As can be seen in Fig. 2, the assembled lattices become less packed from Mg^{2+} to Ca^{2+} to Sr^{2+}. While the individual DNA origami triangles are rather closely spaced within the single-crystalline domains in the presence of Mg^{2+}, their average distance appears slightly increased in the presence of Ca^{2+}. This can be attributed to the reduced association with the DNA phosphates resulting in fewer salt bridges and thus a larger lateral mobility. The even weaker association of Sr^{2+} leads to an even larger average spacing. Here, barely any single-crystalline domains can be observed.

These cation-specific differences in lattice packing lead also to differences in the obtained lattice order. As can be seen in Fig. 2, the fast Fourier transforms (FFTs) of the AFM images of the lattices assembled in the presence of Na^+ exhibit hexagonally shaped correlation rings for both Mg^{2+} and Ca^{2+}. In the case of Ca^{2+}, this correlation ring has a better-defined hexagonal shape and a lower background, both of which are indicative of higher lattice order compared to Mg^{2+}. In the case of Sr^{2+}, however, the FFT shows only a ring without discernible hexagonal shape. This is further quantified in Fig. 3, which

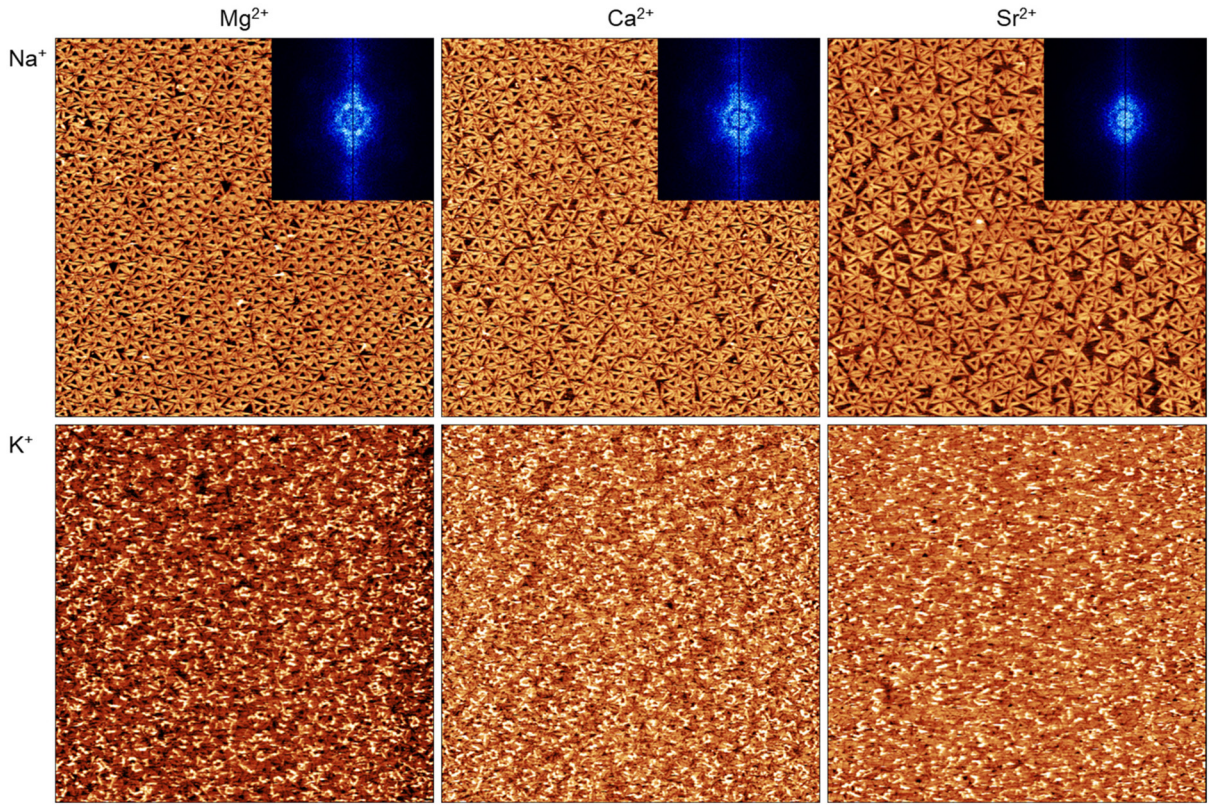

Fig. 2 *In situ* AFM images (3 × 3 μm^2) of DNA lattices assembled from DNA origami triangles at mica surfaces in the presence of different monovalent (90 mM) and divalent cations (10 mM) as indicated. The images were recorded after 60 min incubation. Insets show the fast Fourier transforms (FFTs). For the complete time series, see Fig. S3–S8.

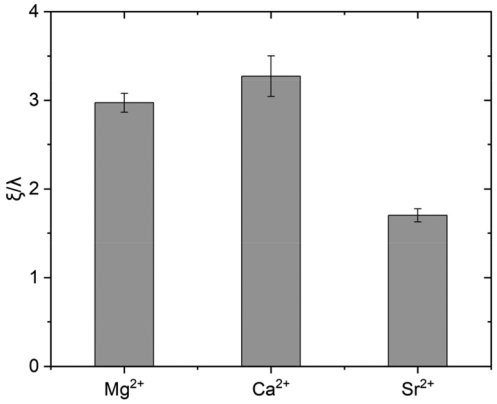

Fig. 3 Relative correlation lengths ξ/λ of the DNA origami lattices obtained in the presence of Na^+ as calculated from the corresponding AFM images shown in Fig. 2.

shows the relative correlation length ξ/λ of each of the three lattices that was calculated from the corresponding AFM images in Fig. 2 and is a measure of the average size of the single-crystalline domains within the polycrystalline lattice.[12,16] In agreement with above qualitative observations, ξ/λ increases by about 10% upon exchanging Mg^{2+} by Ca^{2+}. For Sr^{2+}, however, ξ/λ drops by almost 50%.

At first glance, the trend observed in Fig. 3 may not seem in line with the MD results in Fig. 1. However, just like in other instances of thin-film deposition,[39] lattice order is not a linear function of the lateral mobility of the deposited adatoms or admolecules. In general, three regimes can be identified (Fig. 4):

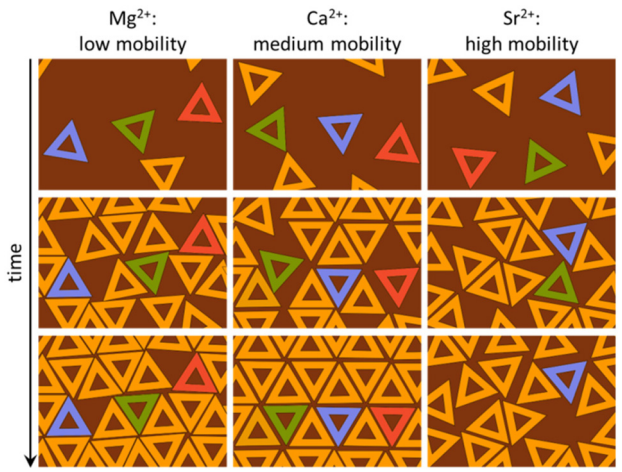

Fig. 4 Schematic representation of the three lattice assembly regimes described in the text. At low DNA origami mobility (Mg^{2+}), the resulting lattice features many defects due to insufficient dynamic annealing. At medium mobility (Ca^{2+}), defects are annealed more efficiently, leading to larger single-crystalline domains. At high mobility (Sr^{2+}), the obtained steady state is dominated by frequent adsorption, diffusion, and desorption events that prevent the formation of a closed monolayer. For each regime, three DNA origami triangles are highlighted in color to visualize their motions.

1. At negligible admolecule mobility, "quenched growth" occurs, which is characterized by large disorder in the deposited film. For crystalline films, this is equivalent to a small average grain size. For DNA origami monolayers, this is usually observed in the absence of monovalent cations.[16] In our experiments, DNA origami mobility is somewhat increased by the presence of Na^+, but the strong binding of the Mg^{2+} ions to the DNA phosphates observed in the MD simulations nevertheless results in comparatively low DNA origami mobility.

2. At medium admolecule mobility, surface diffusion becomes a key factor in determining film structure. In this regime, voids become filled with diffusing admolecules and lattice defects are dynamically annealed by the rearrangement of admolecules in the growing lattice. Increasing admolecule mobility thus leads to a larger average grain size. In our experiments, this is observed in the presence of Ca^{2+} ions, which bind less strongly to the DNA phosphates, resulting in weaker surface interactions and increased DNA origami mobility, so that the obtained lattice exhibits a larger relative correlation length.

3. Increasing the admolecule mobility also leads to an increase in the admolecule desorption rate. At some point, the admolecule desorption rate becomes comparable to the arrival rate at the surface. This leads to a steady-state fractional surface coverage dominated by frequent adsorption, diffusion, and desorption events. In this regime, the film becomes more and more disordered with increasing admolecule mobility. In our experiments, this is observed in the presence of Sr^{2+} ions, which are even more weakly bound than Ca^{2+}. Therefore, the DNA origami surface coverage visible in the AFM images is notably reduced and accompanied by a small relative correlation length.

This nonlinear dependence on DNA origami mobility has already been observed both on mica and SiO_2 surfaces. In the former case, DNA origami mobility was varied by adjusting the Na^+ concentration[16] while in the latter, this was achieved by controlling the surface potential.[21] In the present work, the same behavior is observed upon increasing DNA origami mobility by substituting Mg^{2+} (low mobility) with Ca^{2+} (medium mobility) and with Sr^{2+} (high mobility).

Future investigations may be able to provide more detailed insights into this mechanism and even identify which parameters are ultimately responsible for the observed behavior. High-speed AFM, for example, could be used to determine the surface diffusion coefficients and residence times of different DNA nanostructures at mica and SiO_2 surfaces in the presence of different cation combinations. Here, we settled on evaluating the impacts of charge screening and cation diffusion. We determined the number of positive charges around the DNA by averaging the number of cations (M^+ and M^{2+}) within one Debye length of the experimentally used buffer solution (7.8 Å) from the DNA surface over the MD trajectory (see Table S2). In the presence of Na^+, this results in on average 13.67, 13.43, and 13.00 positive charges for Mg^{2+}, Ca^{2+}, and Sr^{2+}, respectively. Therefore, the difference between Ca^{2+} and Sr^{2+}, *i.e.*, the extreme cases in the

experiments, is less than half a charge. Considering the extremely short Debye length of our buffer and the fact that these simulations were done at a much lower excess of cations to phosphates than the experiments, these minor differences in charge screening can hardly account for the large differences in DNA lattice assembly. Therefore, we next calculated the diffusion coefficients of the different divalent cations (see Table S3). Despite rather large uncertainties, the diffusion coefficient of Sr^{2+} is about twice as large as that of Mg^{2+}, while that of Ca^{2+} is only slightly larger than that of Mg^{2+}. Therefore, these numbers quantitatively reproduce the qualitative observations of Fig. 1. Furthermore, by plotting the experimentally obtained relative correlation lengths *vs.* the diffusion coefficients of the divalent cations obtained from the MD simulations, we define the range of diffusion constants in which we expect to obtain DNA origami lattices with correlation lengths comparable or larger than those obtained in the presence of Mg^{2+} (Fig. S9). This ranges spans from 0.1748×10^{-5} cm^2 s^{-1} to about 0.2227×10^{-5} cm^2 s^{-1} but should be treated with care considering that the uncertainties of the diffusion coefficients are more than ±50% (see Table S3).

In conclusion, we have used MD simulations to investigate the interaction of different combinations of monovalent and divalent cations with DNA. The results were correlated with experimental investigations of the effects of these cation combinations on DNA origami lattice assembly at mica surfaces. Our results reveal that the differential effects of different combinations of monovalent and divalent cations on DNA lattice assembly are rooted in the binding of these cations to DNA. K^+ has a higher affinity for the nucleobases than Na^+, which leads to stronger charge neutralization and in combination with phosphate-bound divalent cations to a local charge inversion. Consequently, DNA origami aggregation and the pile-up of disordered multilayers instead of the formation of ordered lattices is observed in the experiments. For the divalent cations, binding to the DNA phosphates decreases from Mg^{2+} to Ca^{2+} to Sr^{2+}, with weaker binding resulting in higher surface mobility of the adsorbed DNA origami nanostructures. In line with previous experiments at different Na^+ concentrations,[16] lattice order is found to first increase with increasing DNA origami surface mobility (from Mg^{2+} to Ca^{2+}). After reaching a maximum, however, further increases in mobility lead to a decrease in lattice order (from Ca^{2+} to Sr^{2+}). Even though cation-surface interactions may also contribute to this behavior, Mg^{2+}, Ca^{2+}, and Sr^{2+} show rather similar adsorption at mica surfaces.[25,40] Therefore, cation–DNA interactions can be considered a dominant factor governing surface-assisted DNA lattice assembly.

Our results not only provide an explanation for previous experimental observations but also offer a straightforward computational route for screening and selecting suitable cations for surface-assisted DNA lattice assembly. In this context, the determined diffusion coefficients should serve as benchmarks, with divalent cations showing diffusion coefficients around the DNA duplex between 0.1748×10^{-5} cm^2 s^{-1} and 0.2227×10^{-5} cm^2 s^{-1} having great potential for producing highly ordered DNA lattices. Cations outside this range, however, can be expected to yield only low-quality lattices. As an example, Mn^{2+} has an even higher phosphate-binding affinity than Mg^{2+} and thus will probably lead to reduced lattice order.[41] The same may be expected for Ba^{2+}, which shows much weaker phosphate binding than Ca^{2+}.[42] It should be noted, however, that in certain experimental systems, specific cation-surface or DNA-surface interactions may play more dominant roles and possibly outweigh the contributions of cation–DNA interactions.[18,43]

Author contributions

Xiaodan Xu: validation, formal analysis, investigation, visualization, writing – review and editing; Bhanu Kiran Pothineni: methodology, investigation, writing – review and editing; Guido Grundmeier: resources, writing – review and editing, supervision; Satoru Tsushima: conceptualization, methodology, formal analysis, investigation, visualization, writing – original draft, writing – review and editing; Adrian Keller: conceptualization, methodology, visualization, writing – original draft, writing – review and editing, supervision.

Conflicts of interest

There are no conflicts to declare.

Data availability

Data for this article, *i.e.*, raw AFM images and MD simulation files, are available at Zenodo at https://doi.org/10.5281/zenodo.16948456.

Supplementary information (SI): materials and methods, cumulative numbers of cations in the vicinity of base pairs' N and O, typical MD snapshots, AFM images of the complete time series, correlation between correlation length and diffusion coefficient, cumulative coordination number of ions to phosphate, average numbers of cations within the Debye length of the DNA surface, diffusion coefficients of the different divalent cations. See DOI: https://doi.org/10.1039/d5nr03695j.

References

1 S. Ramakrishnan, S. Subramaniam, A. F. Stewart, G. Grundmeier and A. Keller, Regular Nanoscale Protein Patterns via Directed Adsorption through Self-Assembled DNA Origami Masks, *ACS Appl. Mater. Interfaces*, 2016, **8**, 31239–31247.
2 L. Liu, M. Zheng, Z. Li, Q. Li and C. Mao, Patterning Nanoparticles with DNA Molds, *ACS Appl. Mater. Interfaces*, 2019, **11**, 13853–13858.

3 S. Julin, V. Linko and M. A. Kostiainen, Reconfigurable pH-Responsive DNA Origami Lattices, *ACS Nano*, 2023, **17**, 11014–11022.
4 S. Yang, W. Liu, Y. Zhang and R. Wang, Bottom-Up Fabrication of Large-Scale Gold Nanorod Arrays by Surface Diffusion-Mediated DNA Origami Assembly, *ACS Appl. Mater. Interfaces*, 2021, **13**, 50516–50523.
5 D. Mao, L. Liu, C. Zhang, H. Liu and C. Mao, Molecular Lithography on Silicon Wafers Guided by Porous, Extended Arrays of Small DNA Tiles, *Langmuir*, 2023, **39**, 11782–11787.
6 C. Tekin, V. Caroprese and M. M. C. Bastings, Dynamic Surface Interactions Enable the Self-Assembly of Perfect Supramolecular Crystals, *ACS Appl. Mater. Interfaces*, 2024, **16**, 59040–59048.
7 V. Caroprese, C. Tekin, V. Cencen, M. Mosayebi, N. Asmari, T. B. Liverpool, D. N. Woolfson, G. E. Fantner and M. M. C. Bastings, Interface flexibility controls the nucleation and growth of supramolecular networks, *Nat. Chem.*, 2025, **17**, 325–333.
8 L. Liu, Y. Li, Y. Wang, J. Zheng and C. Mao, Regulating DNA Self-assembly by DNA-Surface Interactions, *ChemBioChem*, 2017, **18**, 2404–2407.
9 A. P. Nievergelt, C. Kammer, C. Brillard, E. Kurisinkal, M. M. C. Bastings, A. Karimi and G. E. Fantner, Large–Range HS–AFM Imaging of DNA Self–Assembly through In Situ Data–Driven Control, *Small Methods*, 2019, **3**, 1900031.
10 X. Sun, S. Hyeon Ko, C. Zhang, A. E. Ribbe and C. Mao, Surface-mediated DNA self-assembly, *J. Am. Chem. Soc.*, 2009, **131**, 13248–13249.
11 Y. Xin, X. Ji, G. Grundmeier and A. Keller, Dynamics of lattice defects in mixed DNA origami monolayers, *Nanoscale*, 2020, **12**, 9733–9743.
12 Y. Xin, S. Martinez Rivadeneira, G. Grundmeier, M. Castro and A. Keller, Self-assembly of highly ordered DNA origami lattices at solid-liquid interfaces by controlling cation binding and exchange, *Nano Res.*, 2020, **13**, 3142–3150.
13 Y. Xin, B. Shen, M. A. Kostiainen, G. Grundmeier, M. Castro, V. Linko and A. Keller, Scaling Up DNA Origami Lattice Assembly, *Chem. – Eur. J.*, 2021, **27**, 8564–8571.
14 S. Woo and P. W. K. Rothemund, Self-assembly of two-dimensional DNA origami lattices using cation-controlled surface diffusion, *Nat. Commun.*, 2014, **5**, 4889.
15 A. Aghebat Rafat, T. Pirzer, M. B. Scheible, A. Kostina and F. C. Simmel, Surface-assisted large-scale ordering of DNA origami tiles, *Angew. Chem., Int. Ed.*, 2014, **53**, 7665–7668.
16 C. Kielar, S. Ramakrishnan, S. Fricke, G. Grundmeier and A. Keller, Dynamics of DNA Origami Lattice Formation at Solid-Liquid Interfaces, *ACS Appl. Mater. Interfaces*, 2018, **10**, 44844–44853.
17 B. K. Pothineni, G. Grundmeier and A. Keller, Cation-dependent assembly of hexagonal DNA origami lattices on SiO_2 surfaces, *Nanoscale*, 2023, **15**, 12894–12906.
18 B. K. Pothineni, C. Theile-Rasche, H. Müller, G. Grundmeier, T. de Los Arcos and A. Keller, DNA Origami Adsorption and Lattice Formation on Different SiOx Surfaces, *Chem. – Eur. J.*, 2025, **31**, e202404108.
19 K. Tapio, C. Kielar, J. M. Parikka, A. Keller, H. Järvinen, K. Fahmy and J. J. Toppari, Large-Scale Formation of DNA Origami Lattices on Silicon, *Chem. Mater.*, 2023, **35**, 1961–1971.
20 B. K. Pothineni, J. Barner, G. Grundmeier, D. Contreras, M. Castro and A. Keller, Rapid assembly of highly ordered DNA origami lattices at mica surfaces, *Discover Nano*, 2025, **20**, 77.
21 A. Omoboye, B. K. Pothineni, G. Grundmeier, Z. She and A. Keller, Surface potential-dependent assembly of DNA origami lattices at SiO 2 surfaces, *RSC Appl. Interfaces*, 2025, **2**, 1424–1434.
22 L. Liu, D. Mao, Z. Li, M. Zheng, K. He and C. Mao, Surface-assisted self-assembly of 2D, DNA binary crystals, *Nanoscale*, 2023, **15**, 9941–9945.
23 S. Hamada and S. Murata, Substrate-assisted assembly of interconnected single-duplex DNA nanostructures, *Angew. Chem., Int. Ed.*, 2009, **48**, 6820–6823.
24 S. Adapa, D. R. Swamy, S. Kancharla, S. Pradhan and A. Malani, Role of Mono- and Divalent Surface Cations on the Structure and Adsorption Behavior of Water on Mica Surface, *Langmuir*, 2018, **34**, 14472–14488.
25 M. Ibrahim, C. Wenzel, M. Lallemang, B. N. Balzer and N. Schwierz, Adsorbing DNA to Mica by Cations: Influence of Valency and Ion Type, *Langmuir*, 2023, **39**, 15553–15562.
26 J. Tang, Y. Zhang and S. Bao, The Effect of Ca2+ and Mg2+ on the Dispersion and Flocculation Behaviors of Muscovite Particles, *Minerals*, 2016, **6**, 93.
27 L. Yan, J. H. Masliyah and Z. Xu, Interaction of divalent cations with basal planes and edge surfaces of phyllosilicate minerals: muscovite and talc, *J. Colloid Interface Sci.*, 2013, **404**, 183–191.
28 D. Morzy, R. Rubio-Sánchez, H. Joshi, A. Aksimentiev, L. Di Michele and U. F. Keyser, Cations Regulate Membrane Attachment and Functionality of DNA Nanostructures, *J. Am. Chem. Soc.*, 2021, **143**, 7358–7367.
29 W. He and S. Kirmizialtin, Mechanism of Cationic Lipid Induced DNA Condensation: Lipid-DNA Coordination and Divalent Cation Charge Fluctuations, *Biomacromolecules*, 2024, **25**, 4819–4830.
30 W. He, X. Qiu and S. Kirmizialtin, Sequence-Dependent Orientational Coupling and Electrostatic Attraction in Cation-Mediated DNA-DNA Interactions, *J. Chem. Theory Comput.*, 2023, **19**, 6827–6838.
31 A. Srivastava, R. Timsina, S. Heo, S. W. Dewage, S. Kirmizialtin and X. Qiu, Structure-guided DNA-DNA attraction mediated by divalent cations, *Nucleic Acids Res.*, 2020, **48**, 7018–7026.
32 J. Yoo and A. Aksimentiev, The structure and intermolecular forces of DNA condensates, *Nucleic Acids Res.*, 2016, **44**, 2036–2046.
33 J. Yoo, H. Kim, A. Aksimentiev and T. Ha, Direct evidence for sequence-dependent attraction between double-

stranded DNA controlled by methylation, *Nat. Commun.*, 2016, **7**, 11045.

34 L. Opherden, J. Oertel, A. Barkleit, K. Fahmy and A. Keller, Paramagnetic decoration of DNA origami nanostructures by Eu^{3+} coordination, *Langmuir*, 2014, **30**, 8152–8159.

35 Y. Cheng, N. Korolev and L. Nordenskiöld, Similarities and differences in interaction of K+ and Na+ with condensed ordered DNA. A molecular dynamics computer simulation study, *Nucleic Acids Res.*, 2006, **34**, 686–696.

36 N. V. Hud, F. W. Smith, F. A. Anet and J. Feigon, The selectivity for K+ versus Na+ in DNA quadruplexes is dominated by relative free energies of hydration: a thermodynamic analysis by ^{1}H NMR, *Biochemistry*, 1996, **35**, 15383–15390.

37 Y. Marcus, Thermodynamics of solvation of ions. Part 5.—Gibbs free energy of hydration at 298.15 K, *J. Chem. Soc., Faraday Trans.*, 1991, **87**, 2995–2999.

38 P. W. K. Rothemund, Folding DNA to Create Nanoscale Shapes and Patterns, *Nature*, 2006, **440**, 297–302.

39 D. L. Smith, *Thin-film deposition. Principles and practice*, McGraw-Hill, New York, NY, 1995.

40 S. Adapa and A. Malani, Role of hydration energy and co-ions association on monovalent and divalent cations adsorption at mica-aqueous interface, *Sci. Rep.*, 2018, **8**, 12198.

41 R. M. Clement, J. Sturm and M. P. Daune, Interaction of metallic cations with DNA VI. Specific binding of Mg ++ and Mn ++, *Biopolymers*, 1973, **12**, 405–421.

42 W. Bu, K. Flores, J. Pleasants and D. Vaknin, Preferential affinity of calcium ions to charged phosphatidic acid surface from a mixed calcium/barium solution: X-ray reflectivity and fluorescence studies, *Langmuir*, 2009, **25**, 1068–1073.

43 X. Xu, S. Gołębiowska, T. de Los Arcos, G. Grundmeier and A. Keller, DNA origami adsorption at single-crystalline TiO 2 surfaces, *RSC Appl. Interfaces*, 2025, **2**, 931–939.